ACS OMEGA

Article

Cite This: ACS Omega 2019, 4, 3690−3699

http://pubs.acs.org/journal/acsodf

# Direct Monitoring of Microgel Formation during Precipitation Polymerization of *N*-Isopropylacrylamide Using in Situ SANS

Otto L. J. Virtanen,[†] Michael Kather,[‡,∥] Julian Meyer-Kirschner,[§] Andrea Melle,[†,∥,#] Aurel Radulescu,[⊥] Jörn Viell,[§] Alexander Mitsos,[§] Andrij Pich,[‡,∥] and Walter Richtering*[,†]

[†]Institute of Physical Chemistry, RWTH Aachen University, Landoltweg 2, 52064 Aachen, Germany

[‡]Institute of Technical and Macromolecular Chemistry, RWTH Aachen University, Worringerweg 2, 52074 Aachen, Germany

[§]Aachener Verfahrenstechnik - Process Systems Engineering, RWTH Aachen University, Forckenbeckstr. 51, 52074 Aachen, Germany

[∥]DWI—Leibniz-Institute for Interactive Materials, RWTH Aachen University, Forckenbeckstr. 50, 52056 Aachen, Germany

[⊥]Juelich Centre for Neutron Science (JCNS) at Heinz Maier-Leibnitz Zentrum (MLZ), Forschungszentrum Juelich GmbH, Lichtenbergstr. 1, 85748 Garching, Germany

Supporting Information

**ABSTRACT:** Poly(*N*-isopropylacrylamide) microgels have found various uses in fundamental polymer and colloid science as well as in different applications. They are conveniently prepared by precipitation polymerization. In this reaction, radical polymerization and colloidal stabilization interact with each other to produce well-defined thermosensitive particles of narrow size distribution. However, the underlying mechanism of precipitation polymerization has not been fully understood. In particular, the crucial early stages of microgel formation have been poorly investigated so far. In this contribution, we have used small-angle neutron scattering in conjunction with a stopped-flow device to monitor the particle growth during precipitation polymerization in situ. The average particle volume growth is found to follow pseudo-first order kinetics, indicating that the polymerization rate is determined by the availability of the unreacted monomer, as the initiator concentration does not change considerably during the reaction. This is confirmed by calorimetric investigation of the polymerization process. Peroxide initiator-induced self-crosslinking of *N*-isopropylacrylamide and the use of the bifunctional crosslinker *N*,*N*′-methylenebisacrylamide are shown to decrease the particle number density in the batch. The results of the in situ small-angle neutron scattering measurements indicate that the particles form at an early stage in the reaction and their number density remains approximately the same thereafter. The overall reaction rate is found to be sensitive to monomer and initiator concentration in accordance with a radical solution polymerization mechanism, supporting the results from our earlier studies.

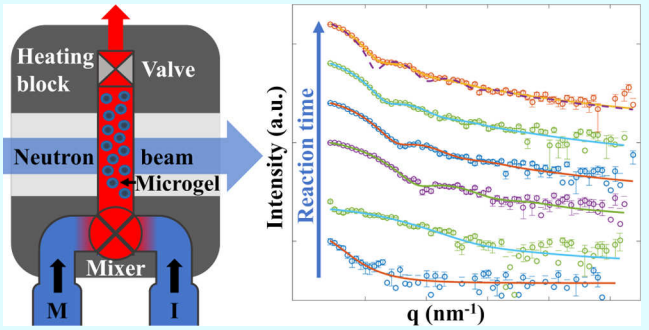


## 1. INTRODUCTION

Poly(*N*-isopropylacrylamide)[1] (PNIPAM) is the most commonly used stimuli-sensitive smart polymer, characterized by its well-defined lower critical solution temperature (LCST) of approximately 32 °C[2] in water. Radical polymerization of aqueous *N*-isopropylacrylamide (NIPAM) solution above the LCST yields soft colloidal particles in the size range of tens of nanometers[3] to a few microns.[4] These so-called microgels[5−7] exhibit a volume phase transition (VPT) at the LCST of PNIPAM and have found various uses, for instance as emulsion stabilizers,[8−11] in membranes,[12−14] for photonics,[15,16] as drug carriers,[17−19] and in bioapplications.[20−26]

Microgels of narrow size distribution are formed during precipitation polymerization of NIPAM.[27,28] The narrow size distribution of these particles, which is also achieved in semibatch and continuous polymerization processes,[29,30] suggests that particle nucleation takes place shortly after initiation and the number of particles remains approximately constant thereafter. This has been attributed to electrostatic stabilization by charged persulfate initiator fragments, which accumulate on the particles as a part of the radical polymerization process.[31] The reaction-condition-dependent chain length has been proposed as the regulating mechanism for the number of stabilizing initiator fragments in the particles.[32,33] Recently, it has been shown that the principles of radical solution polymerization can be effectively used to regulate the stabilization and final particle volume of PNIPAM particles.[34,35]

Received: December 11, 2018
Accepted: February 4, 2019
Published: February 19, 2019






DOI: 10.1021/acsomega.8b03461
ACS Omega 2019, 4, 3690−3699

All these conclusions have been drawn indirectly by investigating the resulting microgel properties. However, to fully understand the formation mechanism of microgels during precipitation polymerization, the early stages of the reaction have to be investigated directly. But, the rapid growth of particles at typical reaction conditions[36] makes the characterization of microgel formation and growth difficult. So far, the investigation of microgel growth has been limited to ex situ experiments, where samples were taken from a batch reactor during polymerization and investigated using dynamic light scattering (DLS).[37] This approach faces the problem that the polymerization process might be disturbed by taking samples out of the batch reactor and the necessity to quench the sample before investigation. Furthermore, this process is time consuming and only a limited amount of samples can be taken at a specific time. Using in situ three-dimensional (3D) DLS, we could monitor the particle growth during the precipitation polymerization of NIPAM under non-stirred conditions.[36] The groups of Wu and Jiang performed similar investigations in two-dimensional DLS for the synthesis of hydroxypropyl cellulose−poly(acrylic acid) and poly(ethylene glycol) dimethacrylate (PEGDMA) microgels.[38,39] In a more recent work, we developed a DLS probe with an automated probe head, allowing the investigation of microgel formation in situ in a batch reactor under stirred conditions.[40] While these setups allowed the undisturbed investigation of particle growth, the temporal resolution was limited to 90 s (3D DLS) respectively 30 s (2D DLS) intervals, preventing the investigation of early stages of the reaction.

The combination of small-angle scattering and stopped-flow techniques allows investigating temporal changes in colloidal systems with great precision.[41−43] In this work, we employ in situ small-angle neutron scattering (SANS) to investigate the effects of monomer, initiator, and crosslinker concentration on the growth of PNIPAM microgels in their native, undisturbed environment with a high temporal resolution of 5 s. High flux SANS in combination with a stopped-flow device for controlled initiation is found to be an ideal tool to track particle and population properties in situ. Combining these techniques, it is possible to investigate the precipitation polymerization of NIPAM in more detail than with previous analytical methods. Understanding the precipitation polymerization in detail is of fundamental interest to polymer chemists and physicists and helps in improving the synthesis methods to customize the smart particles for their numerous applications.

## 2. MODEL EXPRESSION FOR THE SCATTERED INTENSITY

To investigate the effect of monomer, initiator, and crosslinker concentration on microgel formation during the precipitation polymerization of PNIPAM microgels, SANS spectra were taken during polymerization (details of the SANS measurements can be found in the Experimental Section). These spectra are fitted with models described in this section to gain information on the particle volumes and numbers over the course of the polymerization.

In a SANS experiment, the average scattered intensity $I(q)$ from a dispersion of particles is proportional to the structure factor $S(q)$ and form factor $P(q)$, where $q = (4\pi/\lambda) \times \sin(\theta/2)$ denotes the magnitude of the momentum transfer with wavelength $\lambda$ and scattering angle $\theta$.[27]

$$I(q) \propto S(q)P(q) \tag{1}$$

$P(q)$ contains spatially averaged information on the geometry and internal structure of the scatterers; $S(q)$ contributes to the intensity only when the particle positions are correlated. If the interparticle interactions are weak or the dispersion is sufficiently dilute, particle positions in the scattering volume are uncorrelated and $S(q) \to 1$. We shall see that this is the case in the current work (see Figure 1).

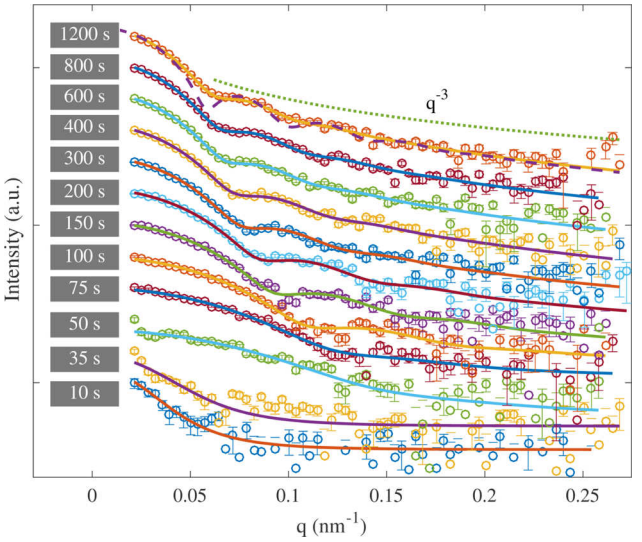


**Figure 1.** Form factors at various reaction times during precipitation polymerization of NIPAM at 65 °C. Solid lines denote the model expression with instrumental smearing. The dashed line shows the model expression without instrumental smearing. The dotted line demonstrates that the scattered intensity decays faster than $q^{-3}$. Datasets are arbitrarily scaled for clear presentation. NIPAM concentration was $2.00 \times 10^{-2}$ mol dm$^{-3}$, ammoniumpersulfate (APS) and *N*,*N*,*N*′,*N*′-tetramethylethylenediamine (TEMED) concentrations were $1.56 \times 10^{-3}$ and $1.56 \times 10^{-3}$ mol dm$^{-3}$, respectively.

For a collection of $n_p$ particles dispersed in scattering volume $V_{sc}$ at nominal scattering vector magnitude $\bar{q}$, the average scattered intensity is given by

$$I(\bar{q}) = \frac{n_p \Delta\rho^2}{V_{sc}} \int_0^\infty \int_0^\infty \mathrm{Res}(\bar{q}, q, \sigma)\mathrm{RDF}(R, \sigma_p)V(R)^2 P(q, R)\mathrm{d}R\ \mathrm{d}q \tag{2}$$

In this expression, $\Delta\rho$ is the scattering contrast between the continuous phase and the particles, $\mathrm{Res}(\bar{q}, q, \sigma)$ is the instrument resolution function, $\mathrm{RDF}(R, \sigma_p)$ is the particle radius distribution function, and $V(R)$ is the scattering weight of the particle fraction with radius $R$. The resolution function can be described by[44,45]

$$\mathrm{Res}(\bar{q}, q, \sigma) = \frac{q}{\sigma^2}\exp\left(-\frac{\bar{q}^2 + q^2}{2\sigma^2}\right) \cdot I_0\left(\frac{\bar{q}q}{\sigma^2}\right) \tag{3}$$

Here $\sigma$ is the smearing parameter for $\bar{q}$, which accounts for the instrument collimation configuration, beam wavelength spread, apertures, and detector pixel size. $I_0(x)$ is the modified Bessel function of the first kind. Pedersen[45] notes that 10 point discretization is sufficient for the calculation of the resolution function. The same discretization was used here.

As the polymerization takes place at a temperature of 65 °C, far above the volume phase transition temperature (VPTT) of



DOI: 10.1021/acsomega.8b03461
ACS Omega 2019, 4, 3690−3699

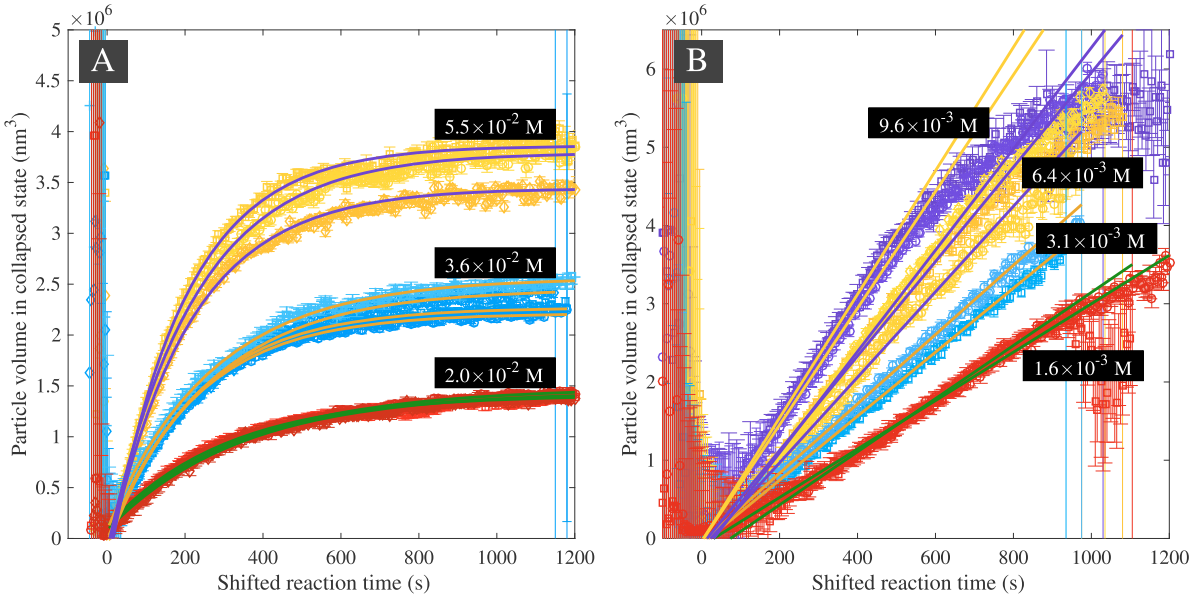


**Figure 2.** Average particle volume with reaction time at 65 °C. Repetitions under the same reaction conditions are denoted by the color scheme. Slight shifts in the traces due to inhibitory effects of oxygen were compensated by shifting the traces to zero reaction time for clear presentation. (A) At various NIPAM concentrations. APS and TEMED were used as redox initiation system. Their concentrations were $1.56 \times 10^{-3}$ and $1.56 \times 10^{-3}$ mol dm$^{-3}$, respectively. Solid lines are fits to eq 11. (B) At various APS concentrations. APS was solely used to initiate the reaction. NIPAM concentration was $3.65 \times 10^{-2}$ mol dm$^{-3}$. Solid lines are linear fits.

PNIPAM, the PNIPAM particles are in a collapsed state. Collapsed PNIPAM particles can be approximated as homogeneous spheres,[27] adequately described by the hard sphere form factor

$$P(q, R) = \left[\frac{3(\sin(qR) - qR\cos(qR))}{(qR)^3}\right]^2 \tag{4}$$

with the scattering weight of a homogenous sphere given by

$$V(R) = \frac{4}{3}\pi R^3 \tag{5}$$

Assuming the particle weight and volume to be distributed according to the normal distribution, it follows that

$$\mathrm{RDF}(R, \sigma_p) = 4\pi^2 g\left(\frac{4}{3}\pi R^3, \sigma_p\right) \tag{6}$$

where $g(V, \sigma_p)$ is the Gaussian distribution with respect to the particle volume and $\sigma_p$ is the polydispersity index, i.e., standard deviation of the distribution divided by its mean. Discretization of 50 points was used in the numerical calculation of the integral over the distribution.

The number of particles formed during the early reaction nucleation period determines the final particle volume of the microgels.[36] Particle nuclei are formed in the early stages of polymerization, probably by a combination of aggregation of precursor particles and adsorption of oligo- and monomers onto precursor particles. After a certain point, these particles are being electrostatically stabilized by the charged initiator fragments, preventing further aggregation of particles.[31] From this point on, the number of particles remains fixed. A model-independent method to approximate the particle number density is the Porod invariant $(Q)$,[46] which is related to the volume fractions of the polymer and heavy water phases in the scattering volume

$$Q = \int_0^\infty I(q)q^2 \mathrm{d}q = 2\pi^2\Phi(1 - \Phi)(\Delta\rho)^2 \tag{7}$$

where $\Phi$ is the volume fraction of polymer in the particle. The unsmeared model expression $I(q)$ was used to calculate the integral. During the reaction, the collapsed polymer is located in particles with average volume $\bar{V}_p$ and therefore the volume fraction of polymer in the scattering volume $V_{sc}$ is given by

$$\Phi = \frac{n_p \Phi_p \bar{V}_p}{V_{sc}} \tag{8}$$

where $\Phi_p$ is the polymer volume fraction inside the particles, here taken as 0.42 for collapsed PNIPAM microgels.[27] The time evolution of the number of particles in the scattering volume can be then approximated by rearranging eq 8 into

$$n_p(t) = \frac{\Phi(t)V_{sc}}{\Phi_p \bar{V}_p(t)} \tag{9}$$

## 3. RESULTS AND DISCUSSION

**3.1. Validity of the Model Expression.** Typical data from in situ stopped-flow polymerization at various reaction times is shown in Figure 1. After initiation of the polymerization in the mixer chamber, the reaction mixture is rapidly directed to the observation cuvette, where it remains stationary during the reaction. The early reaction time scattering pattern is typically flat, except for a sharp upturn at the low $q$ region. Strong forward scattering indicates the presence of large structures. The origin of this phenomenon is likely due to small argon bubbles from mixing, as any polymer structures present at the early reaction stage are expected to be small. With increasing reaction time, scattering from growing polymer particles begins to dominate the scattered intensity. This is seen from the emergence of a form factor minimum, which shifts to smaller $q$ values with increasing particle size.



DOI: 10.1021/acsomega.8b03461
ACS Omega 2019, 4, 3690−3699

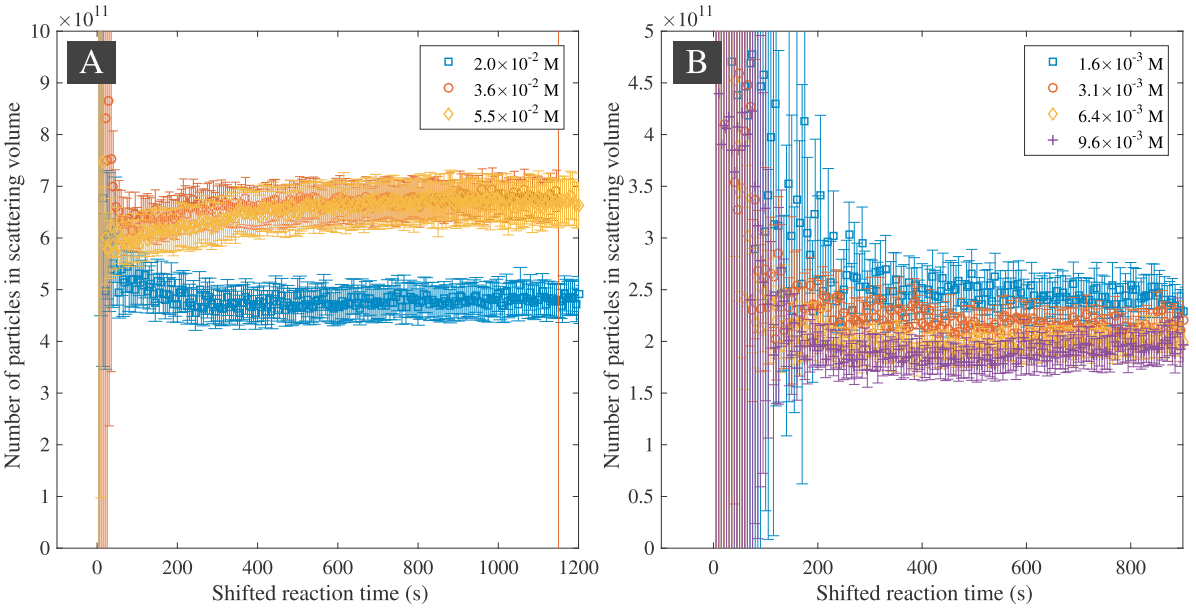


**Figure 3.** Number of particles with reaction time, averaged over repetitions. (A) At various NIPAM concentrations. APS and TEMED concentrations were $1.56 \times 10^{-3}$ and $1.56 \times 10^{-3}$ mol dm$^{-3}$, respectively. Solid lines are fits to eq 11. (B) At various APS concentrations. No TEMED was used in these syntheses. NIPAM concentration was $3.65 \times 10^{-2}$ mol dm$^{-3}$.

Solid lines in Figure 1 denote the model expression, eq 2, fitted to the data points. Generally, the model captures well the data features, confirming that collapsed PNIPAM particles can be treated as homogeneous spheres. A homogeneous structure is to be expected as the thermal blobs of a polymer in a poor solvent, such as PNIPAM at temperatures above the volume phase transition temperature (VPTT) in $D_2O$, pack densely together to minimize the surface area with the solvent.[47] For reference, the dotted line above the upmost form factor shows the unsmeared scattering pattern without instrumental effects.

The calculation of the Porod invariant imposes certain requirements for the system under investigation.[46] The experimental intensity should not exhibit a strong upturn as $q \to 0$, which is typical for aggregated systems. In addition, the scattering intensity has to decay faster than $q^{-3}$. In our experiment, smooth behavior and good model fit in the low $q$ regime of the experimental data indicate that no aggregation of particles takes place during polymerization. Aggregation would be observed as intensified forward scattering and/or a kink in the low $q$ regime due to correlation of particle positions in a small aggregate, in analogy to the structure factor. In fact, the data show no evidence of a structure factor contribution in the experimentally accessible $q$ range, which indicates dilute dispersion and/or weak interactions between the particles. The model used here would not be able to describe these features if they were present, leading to a poor fit. Comparing experimental data to the dotted line shows that the experimental data decay faster than $q^{-3}$, fulfilling the other requirement.

**3.2. Particle Growth Follows Pseudo-First-Order Kinetics.** Monomer and initiator concentration have considerable effects on the final particle volume of PNIPAM microgels, which exhibits power law behavior with respect to both of these reactants.[34,35] In situ 3D dynamic light scattering experiments have shown the average growth rate of the particles to increase with both the monomer and initiator concentration.[36] Figure 2A confirms that the average volume growth rate and final particle volume are strongly influenced by the initial monomer concentration. Identically colored traces denote measurement repetition under identical reaction conditions. Slightly variable induction periods were observed for the repeated measurements, presumably caused by trace amounts of oxygen in the instrument. Due to this, all traces shown in Figure 2 are shifted to zero reaction time to compensate for the inhibitory effect of the oxygen and allow for a better comparison of reactions repeated at the same reaction conditions. The experiment is found to be most reproducible at the lowest monomer concentration of $2.0 \times 10^{-2}$ mol dm$^{-3}$. In contrast, experiments with the higher monomer concentration show more variation with respect to the final particle volume. The high initial volumes with large uncertainty possibly arise from microbubbles as discussed in the context of Figure 1.

PNIPAM microgels typically have a narrow size distribution,[27,28] which implies a short particle nucleation phase at the beginning of the reaction and subsequent particle growth. If new particles would be formed in later stages of the reaction, broadening of the particle size distribution would be expected, as new particle nuclei would form alongside the already growing microgel particles. These new particles would either form new microgels, increasing the number of particles during the polymerization, or aggregate onto existing microgel particles. In either case, it would cause an increase in particle size distribution that does not fit to the observed narrow size distribution for PNIPAM. If no particle aggregation takes place during the polymerization, the time evolution of the average particle volume during the reaction can be assumed as follows

$$\bar{V}_p(t) = \frac{V_M}{n_p(t)} \int_0^t R_p(t)\mathrm{d}t \tag{10}$$

where $V_M$ is the volume of the collapsed polymer, including water,[48] polymerized from one mole of NIPAM, $n_p$ is the number of particles in the batch, and $R_p$ is the rate of monomer consumption. The experimentally observed particle growth in Figure 2A could be well described with an equation of the form



DOI: 10.1021/acsomega.8b03461
ACS Omega 2019, 4, 3690−3699

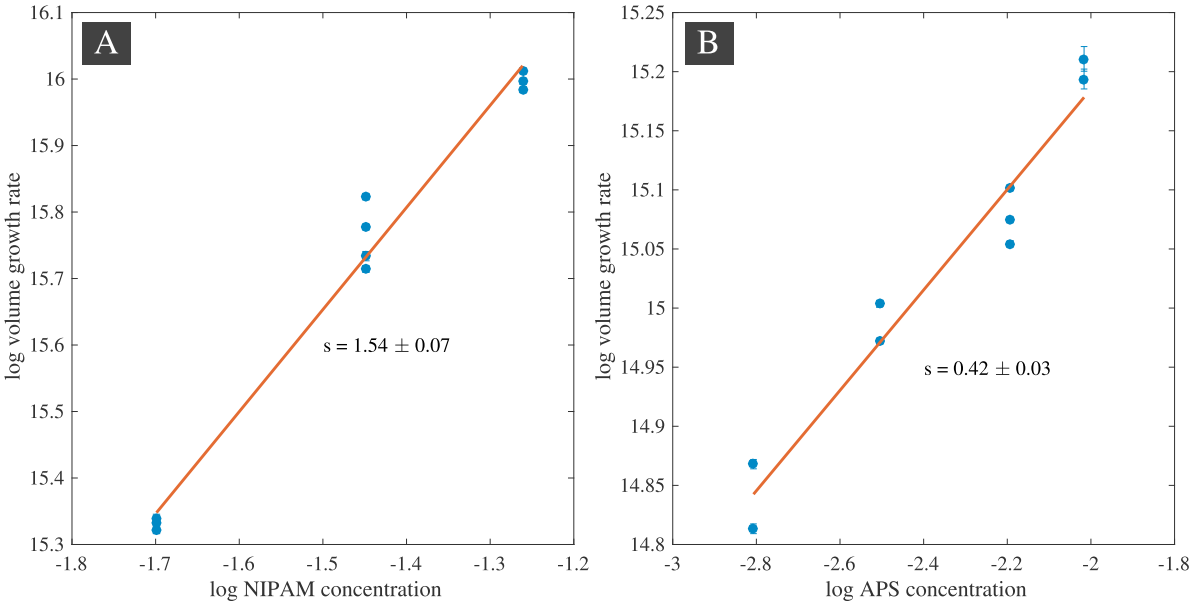


**Figure 4.** Total volume growth rate extrapolated to zero time in log−log presentation. (A) Plotted against varying NIPAM concentration. APS and TEMED were used as redox initiation system. Their concentrations were $1.56 \times 10^{-3}$ and $1.56 \times 10^{-3}$ mol dm$^{-3}$, respectively. (B) Plotted against varying APS concentration. No TEMED was used in these syntheses. NIPAM concentration was $3.65 \times 10^{-2}$ mol dm$^{-3}$. Solid lines denote linear fit to the data points.

$$\bar{V}_p(t) = \frac{V_M}{n_p}\left[1 - \exp\left(-\frac{t}{\tau}\right)\right] \quad (11)$$

where $\tau$ is the time constant of the reaction. Single exponential behavior implies that the particle growth rate depends only on monomer concentration, indicating pseudo-first-order kinetics for polymerization. Furthermore, the observed behavior requires the particle concentration to remain approximately constant throughout the growth phase. Similar results have been reported by Wu et al. for poly(ethylene glycol) dimethacrylate (PEGDMA) nanogels crosslinked with divinylbenzene.[39]

Pseudo-first-order behavior can take place if the initiator concentration does not change considerably during the reaction due to the long half-life time of the initiator. Under these conditions, the initiator concentration can be assumed to be constant so that the reaction kinetics depend only on the monomer concentration.[49] Polymerization was initiated with an APS−TEMED system to minimize the effects of oxygen in the stopped-flow instrument. Peroxide−amine redox initiation is typically 1−3 orders of magnitude faster than the corresponding peroxide without the accelerator[50] and rapidly consumes any trace amounts of oxygen in the stopped-flow cuvette. Assuming that the rate constant for the redox reaction is of the order of $1.2 \times 10^{-2}$ dm$^3$ mol$^{-1}$ s$^{-1}$,[50] the half-lives of the redox components are approximately 14 h, given that the concentration of $1.56 \times 10^{-3}$ mol dm$^{-3}$ is used for both APS and TEMED. The volume traces in Figure 2A approach a plateau after 20 min of reaction time, showing that the time necessary to approach full conversion is short in comparison with the initiator half-life. This result supports the notion that the pseudo-first-order kinetics arise from negligible initiator consumption.

Particle growth traces for pure APS initiation without the accelerator TEMED are shown in Figure 2B. These syntheses were performed without TEMED to investigate the influence of initiator concentration on particle growth while simultaneously investigating the effect of initiator-induced self-crosslinking of NIPAM on particle number density (Figure 3). Although TEMED was used during precipitation polymerization at varying monomer concentrations (Figure 2A), it should not strongly affect the results in comparison to the effect of initiator concentration (Figure 2B), as radical initiators were used in both cases.

Long and variable induction periods were observed with the thermally decomposing initiator. The instrument was always flushed with argon-purged $D_2O$ to remove oxygen from the system prior to loading the deoxygenized reactants to the stopped-flow device. Despite intensive flushing, trace amounts of oxygen in the instrument are the most likely explanation for the initial inhibition of the reaction.

The reaction rate was significantly reduced without the accelerator TEMED, which is seen from the fact the particle volume trace does not level off in a comparable polymerization time frame as in Figure 2A. The initial particle growth regime appears to be linear for all except the highest APS concentration of $9.6 \times 10^{-3}$ mol dm$^{-3}$. The same behavior has been reported earlier for in situ 3D DLS measurements using potassium persulfate (KPS) as the initiator.[36] The traces in Figure 2B were fitted with a linear model. For the highest APS concentration, the fit was limited to the linear section of the trace.

**3.3. Evolution of Particle Number Density with Reaction Time.** The number of particles with reaction time was calculated from eq 9 for batches with variable NIPAM and APS concentration, shown in Figure 3A,B, respectively. In all cases, the number of particles in the scattering volume approaches a plateau, confirming that the particle number density remains approximately constant throughout the reaction. The apparent particle number in scattering volume is also affected by possible sedimentation of particles and convection due to temperature gradients in the stopped-flow instrument. Given the scattering volume of $4.8 \times 10^{-5}$ dm$^3$, all particle concentrations in this work settle in the range of $10^{15}$−



DOI: 10.1021/acsomega.8b03461
ACS Omega 2019, 4, 3690−3699

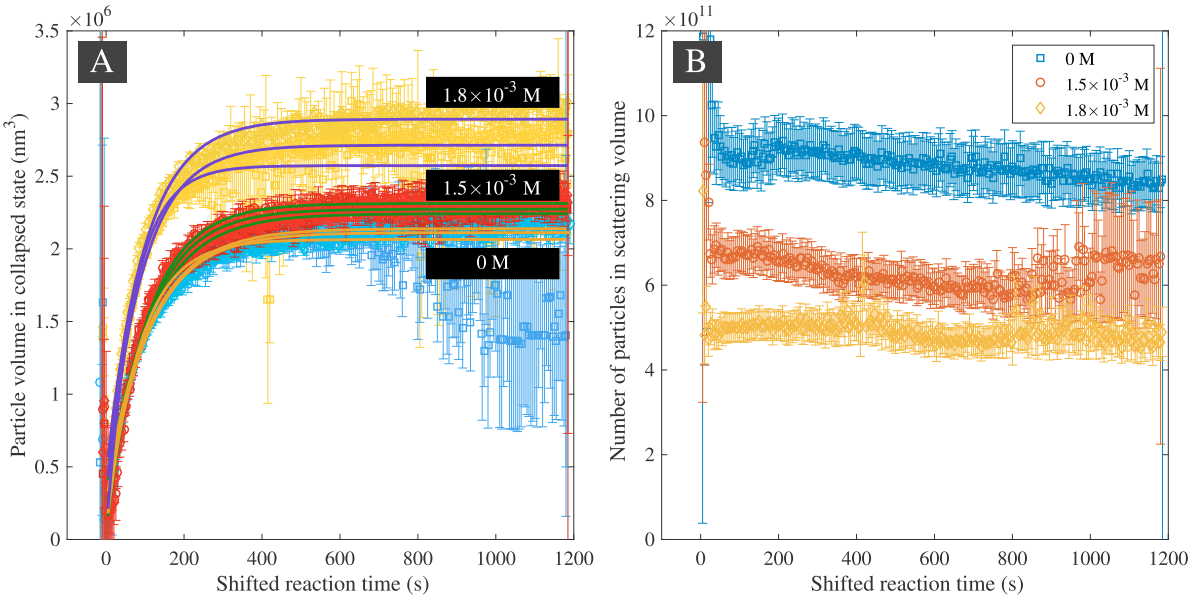


**Figure 5.** (A) Average particle volume with reaction time with increasing bisacrylamide concentration. Repetitions with the same reaction conditions are denoted by the color scheme. Slight shifts in the traces due to inhibitory effects of oxygen were compensated by shifting the traces to zero reaction time for clear presentation. In each batch, NIPAM concentration was $3.65 \times 10^{-2}$ mol dm$^{-3}$, APS concentration was $1.56 \times 10^{-3}$ mol dm$^{-3}$, and TEMED concentration was $3.12 \times 10^{-3}$ mol dm$^{-3}$. BIS concentrations are given in the graph. (B) Number of particles with increasing bisacrylamide concentration.

$10^{16}$ dm$^{-3}$, which is compatible with values of $10^{15}$–$10^{17}$ dm$^{-3}$ reported earlier by Wu et al.[31]

For three different NIPAM concentrations in Figure 3, the final particle concentration varies in a nonlinear way. This is consistent with earlier findings which indirectly showed that the particle concentration at the end of the reaction ($n_p$) depends on the initial NIPAM concentration in the batch. In a series of batches with increasing NIPAM concentration, the end particle concentration first increases, goes through a maximum, and then decreases.[34,35]

Peroxide initiators (used without accelerator) are known to induce crosslinking of PNIPAM chains to the extent that microgels are formed even without an additional crosslinker.[32,33] Recently, we have shown that the crosslinks concentrate at the particle periphery, leading to an inverted crosslinking structure in comparison to conventional PNIPAM microgels.[28] The particle volume in the collapsed state has been shown to increase with KPS concentration,[33,36] which can be attributed to either decreasing particle concentration or increasing water affinity of the network due to the increased number of hydrophilic initiator fragments.

Figure 3B shows a systematically decreasing number of particles in the scattering volume with increasing APS concentration. If the polymer volume fraction $\Phi_p$ within the particles decreased due to increased water affinity, the apparent number of particles should increase according to eq 9. As the opposite behavior is observed in Figure 3B, we conclude that the particle number density does indeed decrease with increasing peroxide initiator concentration. Previous work has shown that the increased ionic strength due to peroxide initiator does not significantly promote the coagulation of the nuclei[34] and therefore the likely explanation for the decreased particle density is the increased probability of irreversible nuclei aggregation due to peroxide-induced self-crosslinking reactions.

**3.4. Total Volume Growth Rate is Proportional to the Polymerization Rate.** Rearrangement of eq 10 shows that the total volume growth rate is proportional to the polymerization rate up to a constant factor $V_M^{-1}$ as

$$R_p(t) \propto n_p(t) \frac{d\,\bar{V}_p}{dt} \tag{12}$$

Figure 4 shows the total volume growth rate with NIPAM and APS concentration. The total volume growth rate increases when both the monomer and initiator concentration in the batch is increased, being clearly more sensitive to NIPAM concentration in comparison to APS concentration. Earlier studies have shown the polymerization rate to be close to the power law behavior of radical solution polymerization with $R_p \propto [\text{monomer}][\text{initiator}]^{1/2}$ shortly after initiation.[35,36] This is not surprising, given the abundant solubility of NIPAM in water, which implies that significant conversion takes place in the water phase during early reaction stages.

The power law exponent with respect to NIPAM concentration, determined here as 1.54 ± 0.07, is higher than expected based on the earlier results of 0.94 ± 0.08[36] and 1.05 ± 0.08.[35] However, given the limited amount of experimental data, the value is in reasonable agreement with previous work. As expected for radical solution polymerization, the power law exponent of 0.42 ± 0.03 in respect to APS concentration is close to half an order of magnitude lower than for the NIPAM concentration. This result is in good agreement with earlier results of 0.46 ± 0.05[36] and 0.56 ± 0.03.[35]

**3.5. Effect of Crosslinker Bisacrylamide on Particle Growth Rate and Number Density.** *N*,*N*′-methylenebisacrylamide (BIS) is a typical crosslinker employed for the synthesis of microgels. Copolymerization with BIS increases the particle size of microgels in the collapsed state, which has been documented on multiple occasions.[31,33−35] Figure 5A shows that even a small addition of BIS to the monomer



DOI: 10.1021/acsomega.8b03461
ACS Omega 2019, 4, 3690−3699

mixture has a considerable effect on the average particle growth, leading to larger final particle volume.

The low amounts of BIS used in the syntheses do not significantly alter the water affinity of the network. Therefore, the likely explanation for the increased particle size is a decrease in the particle number density. This is confirmed in Figure 5B, which shows the decrease of particle number in the scattering volume with increasing BIS concentration.

As the number of particles in the scattering volume remains approximately constant throughout the reaction, the differences in the number of particles arise already at the onset of the reaction during the nucleation phase. Incorporation of bifunctional bisacrylamide units to the nuclei increase the probability of their irreversible aggregation with each other, which leads to a decrease in the particle number density.

The effect of BIS on the total volume growth rate of the particles was calculated from eq 12 (Supporting Information (SI): Figure S1). Even though BIS clearly decreases the number of particles in the batch, leading to larger final particle volume, the effect on the reaction rate is less pronounced. Therefore, the reactions were repeated in a reaction calorimeter. The measured reaction heat is mainly due to the cleavage of the NIPAM double bonds, which is directly proportional to the reaction rate. In the resulting calorigrams in Figure 6, a slight influence of BIS concentration on the reaction rate can be observed. The reaction rate increases slightly in the reaction beginning with increasing BIS concentration, resulting in a higher heat output and stronger peak intensity. Still, the overall duration of the reaction remains the same, as the crosslinker is consumed faster than NIPAM. Additionally, the total conversion increases with rising BIS concentration. This can be attributed to a bigger influence of the crosslinker on the total reaction enthalpy with increasing BIS concentration.

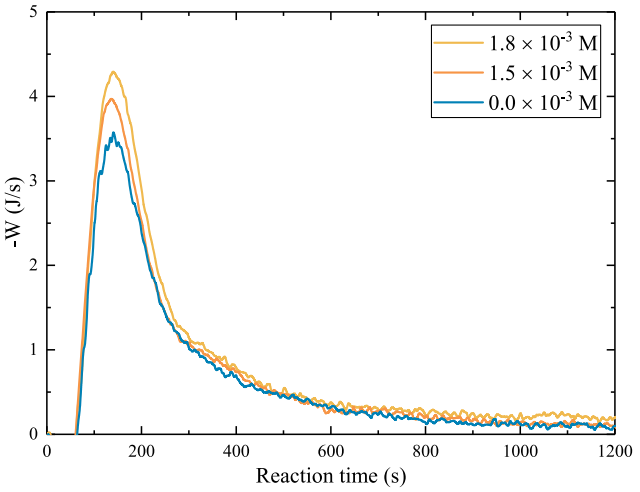


**Figure 6.** Calorigrams for PNIPAM microgel syntheses with increasing BIS concentration. In each batch, the NIPAM concentration was 3.65 × $10^{-2}$ mol $dm^{-3}$, APS concentration was 1.56 × $10^{-3}$ mol $dm^{-3}$, and TEMED concentration was 3.12 × $10^{-3}$ mol $dm^{-3}$. BIS concentrations are given in the graph.

Using the heat of polymerization of NIPAM, determined to be 84.5 ± 0.3 kJ $mol^{-1}$ in one of our previous reports,[35] it is possible to calculate the conversion depending on the reaction time (Figure 7A). Performing a single exponential fit of the conversion data with eq 11 on the NIPAM synthesis without BIS shows a good agreement with corresponding fits of the scattering data (Figure 5). But as soon as BIS is added to the reaction, the fit shows nonsingle exponential behavior. This is to be expected, since the reaction proceeds with copolymerization kinetics as soon as the bifunctional monomer BIS is added to the reaction. A two exponential equation (SI: eq S1) is used to incorporate those kinetics, resulting in a better agreement with the experimental data (single plots can be found in SI Figure S2). Using these fits, the initial reaction rates ($r_{initial}$) can be determined (for details, see SI), showing an increase in the initial reaction rate with increasing BIS concentration (Figure 7B). These results are in agreement with our earlier findings by a combination of experimental and simulation results for poly(*N*-vinylcaprolactam) (PVCL) and PNIPAM microgels.[51,52] Furthermore, Wu and Pelton documented similar findings, showing that the reaction rate of BIS is higher than that of NIPAM.[51]

In summary, these calorimetry results are in agreement with the scattering results, confirming that monomer concentration controls the reaction rate. This effect is less pronounced in the scattering data, which can be attributed to a higher error in the scattering experiments.

## 4. CONCLUSIONS

In this work, we monitored the particle growth in the precipitation polymerization of *N*-isopropylacrylamide in situ by small-angle neutron scattering (SANS). In earlier work, features of the reaction have been deduced from the properties of the resulting polymer particles; here, we presented data from direct measurements throughout the evolution of growing microgels.

The average particle volume growth was found to adhere to pseudo-first-order kinetics, indicating that the polymerization rate is dominated by the amount of unreacted monomer at any given reaction state. Scattering data showed that monomer, initiator, and crosslinker concentration all affect the particle number density in the batch, which in turn determines the final particle volume. Of special note is the effect of crosslinking reactions: both persulfate initiator-induced crosslinking and the bifunctional monomer decrease the concentration of particles in the batch, presumably because of increased probability of irreversible aggregation of particle nuclei during the nucleation phase.

Spherical particles could be detected rapidly after the reaction onset, after which the particle concentration remained approximately constant. The initial polymerization rate deduced from the total volume growth rate in the reaction was sensitive to both initiator and monomer concentration, in accordance to the radical solution mechanism. In case of the crosslinker concentration, the effect on the initial polymerization rate could not be conclusively determined using SANS, due to the low amount of crosslinker used for the polymerization. In combination with calorimetry, however, it could be shown that the crosslinker has a slight influence on the initial reaction rate. The in situ measurements presented in this article not only confirm the earlier studies that relied on indirect measurements but further solidify our understanding of precipitation polymerization of thermosensitive polymers.

Finally, we demonstrate that stopped-flow SANS, in combination with sophisticated automated fitting routines that allow analyzing large datasets, provides new opportunities to investigate colloidal systems under nonequilibrium conditions. These techniques will be developed further by



DOI: 10.1021/acsomega.8b03461
*ACS Omega* 2019, 4, 3690−3699

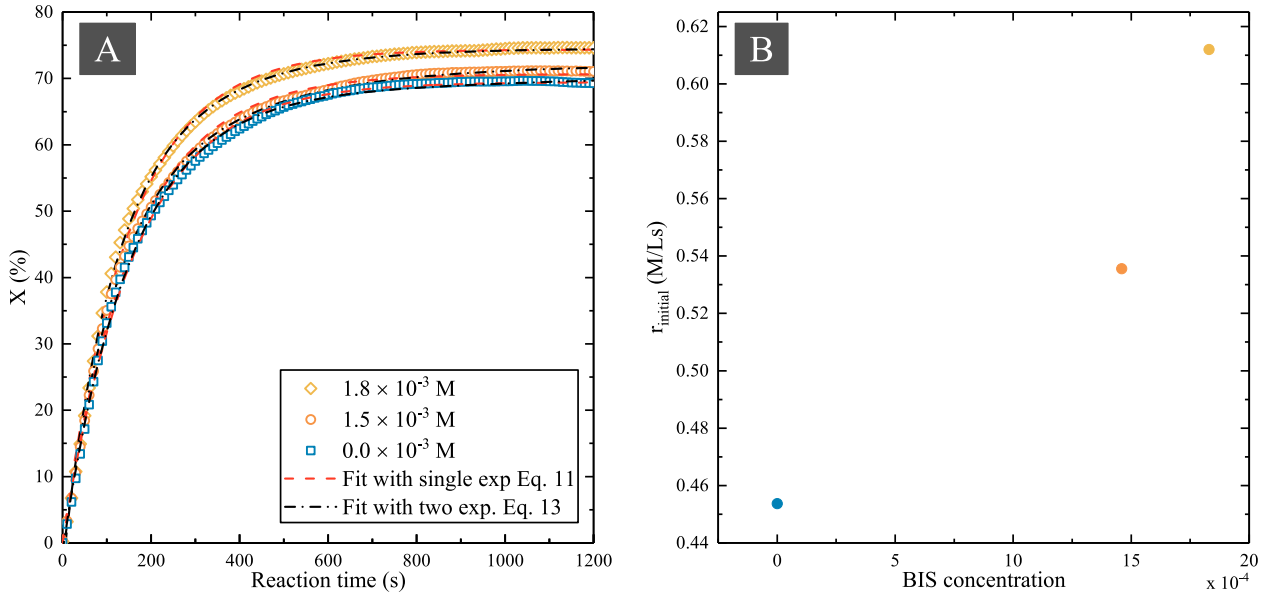


**Figure 7.** (A) Conversion during the precipitation polymerization of PNIPAM depending on the reaction time, fitted with the single exponential eq 11 and the two exponential eq S1. (B) Initial reaction rates in dependence of BIS concentration.

exploring contrast variation to provide additional detailed information on the structure of complex colloids.

## 5. EXPERIMENTAL SECTION

**5.1. Small-Angle Neutron Scattering (SANS).** All in situ measurements were performed at the small-angle neutron scattering diffractometer KWS-2[53] at a detector distance of 20 m. The instrument resolution was determined by a 20% wavelength spread of the neutron beam. Precipitation polymerization was initiated in a BioLogic SFM-300 stopped-flow device, which was positioned in the neutron beam (Figure 8). SFM-300 was connected to a Julabo refrigerated circulator set to a temperature of 65 °C.

NIPAM was recrystallized from hexane; the crosslinker *N*,*N*′-methylenebisacrylamide (BIS), initiator ammoniumpersulfate (APS), and accelerator *N*,*N*,*N*′,*N*′-tetramethylethylenediamine (TEMED) were used as received. Separate monomer and initiator solutions of appropriate concentrations were prepared in heavy water and deoxygenized by purging with argon. When the accelerator TEMED was used, it was mixed directly with the monomers. Prior to loading the monomer and initiator into separate sample chambers of the SFM-300 instrument, the chambers, channels, mixer, and cuvette were flushed with deoxygenized heavy water to remove oxygen from the device.

After tempering the monomer and initiator solutions in the chambers for at least 15 min, the reaction was initiated by rapidly mixing the monomer and initiator in 1:1 ratio at 65 °C. The reaction was monitored for minimum 20 min, using 5 s integration time.

Program FitIt!,[a] was scripted to fit approximately 15 000 datasets from 3 individual syntheses with the model described in the previous section.

**5.2. Calorimetry.** To measure the heat transferred during the polymerization of NIPAM monomers by the cleavage of the double bonds, an RC1su reaction calorimeter with a triple-walled 500 mL RTCal glass reactor from Mettler Toledo was used. The measuring principles have previously been reported in the literature.[54,55] The calorimeter was operated in the

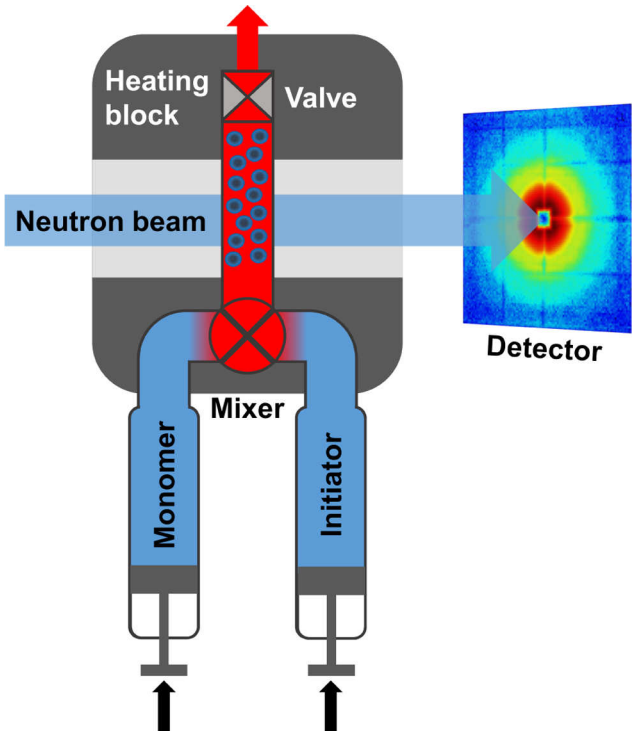


**Figure 8.** Experimental setup of the BioLogic SFM-300 stopped-flow device in the neutron beam.

isothermal mode, meaning that the reaction temperature $T_r$ was set to a constant value of 60 °C, whereas the jacket temperature $T_j$ changed automatically to maintain a constant $T_r$. The enthalpy of polymerization is measured by monitoring the heat transfer rate between the reaction vessel and the heating jacket using a thermocouple embedded in the polymer matrix in the inner glass wall of the jacket. The reaction heat curve is obtained with a resolution of 2 s between the measurements. The polymerization was carried out using 300 mL of reaction mixture. NIPAM, BIS, and TEMED were dissolved in double-distilled water inside the glass reactor,



DOI: 10.1021/acsomega.8b03461
ACS Omega 2019, 4, 3690−3699

purged with argon for 30 min, and equilibrated for 30 min under stirring (100 rpm) to the desired reaction temperature. To initiate the polymerization, a preheated degassed solution of APS in 2 mL of double-distilled water was added rapidly through a 3 mL syringe into the reactor.

## ■ ASSOCIATED CONTENT

### Supporting Information

The Supporting Information is available free of charge on the ACS Publications website at DOI: 10.1021/acsomega.8b03461.

Plots of the volume growth rate depending on the BIS concentration, fit functions for determination of the initial reaction rate, and conversion plots over time fitted with the initial reaction rate fit function (PDF)

## ■ AUTHOR INFORMATION


### Corresponding Author

*E-mail: wrichtering@pc.rwth-aachen.de.

### ORCID

Jörn Viell: 0000-0003-0587-6151

Alexander Mitsos: 0000-0003-0335-6566

Andrij Pich: 0000-0003-1825-7798

Walter Richtering: 0000-0003-4592-8171

### Present Address

[#]Klinik und Polilkinik für Nuklearmedizin, Klinikum rechts der Isar, Technical University of Munich, Ismaninger Str. 22, 81675 Munich, Germany (A.M.).


### Notes

The authors declare no competing financial interest.

## ■ ACKNOWLEDGMENTS

This work was supported by the Deutsche Forschungsgemeinschaft within the SFB 985 "Functional Microgels and Microgel Systems".

## ■ ADDITIONAL NOTE

[a]https://github.com/ovirtanen/fitit.

## ■ REFERENCES


(1) Schild, H. G. Poly(*N*-isopropylacrylamide): Experiment, Theory and Application. *Prog. Polym. Sci.* **1992**, *17*, 163−249.

(2) Halperin, A.; Kröger, M.; Winnik, F. M. Poly(*N*-isopropylacrylamid)-Phasendiagramme: 50 Jahre Forschung. *Angew. Chem.* **2015**, *127*, 15558−15586.

(3) McPhee, W.; Tam, K. C.; Pelton, R. Poly(*N*-isopropylacrylamide) latices prepared with sodium dodecyl sulfate. *J. Colloid Interface Sci.* **1993**, *156*, 24−30.

(4) Meng, Z.; Smith, M. H.; Lyon, L. A. Temperature-programmed synthesis of micron-sized multi-responsive microgels. *Colloid Polym. Sci.* **2009**, *287*, 277−285.

(5) Pelton, R. Temperature-sensitive aqueous microgels. *Adv. Colloid Interface Sci.* **2000**, *85*, 1−33.

(6) Pich, A.; Richtering, W. *Chemical Design of Responsive Microgels*; Springer, 2010; pp 1−37.

(7) Plamper, F. A.; Richtering, W. Functional Microgels and Microgel Systems. *Acc. Chem. Res.* **2017**, *50*, 131−140.

(8) Wiese, S.; Spiess, A. C.; Richtering, W. Microgel-Stabilized Smart Emulsions for Biocatalysis. *Angew. Chem.* **2013**, *125*, 604−607.

(9) Schmitt, V.; Ravaine, V. Surface compaction versus stretching in Pickering emulsions stabilised by microgels. *Curr. Opin. Colloid Interface Sci.* **2013**, *18*, 532−541.

(10) Deshmukh, O. S.; van den Ende, D.; Stuart, M. C.; Mugele, F.; Duits, M. H. Hard and soft colloids at fluid interfaces: Adsorption, interactions, assembly & rheology. *Adv. Colloid Interface Sci.* **2015**, *222*, 215−227.

(11) Wellert, S.; Richter, M.; Hellweg, T.; von Klitzing, R.; Hertle, Y. Responsive Microgels at Surfaces and Interfaces. *Z. Phys. Chem.* **2015**, *229*, 1225−1250.

(12) Menne, D.; Pitsch, F.; Wong, J. E.; Pich, A.; Wessling, M. Temperature-Modulated Water Filtration Using Microgel-Functionalized Hollow-Fiber Membranes. *Angew. Chem., Int. Ed.* **2014**, *53*, 5706−5710.

(13) Roghmans, F.; Martí-Calatayud, M.; Abdu, S.; Femmer, R.; Tiwari, R.; Walther, A.; Wessling, M. Electrochemical impedance spectroscopy fingerprints the ion selectivity of microgel functionalized ion-exchange membranes. *Electrochem. Commun.* **2016**, *72*, 113−117.

(14) Lohaus, T.; de Wit, P.; Kather, M.; Menne, D.; Benes, N.; Pich, A.; Wessling, M. Tunable permeability and selectivity: Heatable inorganic porous hollow fiber membrane with a thermo-responsive microgel coating. *J. Membr. Sci.* **2017**, *539*, 451−457.

(15) Gao, Y.; Li, X.; Serpe, M. J. Stimuli-responsive microgel-based etalons for optical sensing. *RSC Adv.* **2015**, *5*, 44074−44087.

(16) Go, D.; Rommel, D.; Chen, L.; Shi, F.; Sprakel, J.; Kuehne, A. J. Programmable Phase Transitions in a Photonic Microgel System: Linking Soft Interactions to a Temporal pH Gradient. *Langmuir* **2017**, *33*, 2011−2016.

(17) Hoare, T. R.; Kohane, D. S. Hydrogels in drug delivery: Progress and challenges. *Polymer* **2008**, *49*, 1993−2007.

(18) Merkel, T. J.; Jones, S. W.; Herlihy, K. P.; Kersey, F. R.; Shields, A. R.; Napier, M.; Luft, J. C.; Wu, H.; Zamboni, W. C.; Wang, A. Z.; Bear, J. E.; DeSimone, J. M. Using mechanobiological mimicry of red blood cells to extend circulation times of hydrogel microparticles. *Proc. Natl. Acad. Sci. U.S.A.* **2011**, *108*, 586−591.

(19) Schmid, A. J.; Dubbert, J.; Rudov, A. A.; Pedersen, J. S.; Lindner, P.; Karg, M.; Potemkin, I. I.; Richtering, W. Multi-Shell Hollow Nanogels with Responsive Shell Permeability. *Sci. Rep.* **2016**, *6*, No. 22736.

(20) Brown, A. C.; Stabenfeldt, S. E.; Ahn, B.; Hannan, R. T.; Dhada, K. S.; Herman, E. S.; Stefanelli, V.; Guzzetta, N.; Alexeev, A.; Lam, W. A.; Lyon, L. A.; Barker, T. H. Ultrasoft microgels displaying emergent platelet-like behaviours. *Nat. Mater.* **2014**, *13*, 1108.

(21) Sigolaeva, L. V.; Gladyr, S. Y.; Gelissen, A. P.; Mergel, O.; Pergushov, D. V.; Kurochkin, I. N.; Plamper, F. A.; Richtering, W. Dual-Stimuli-Sensitive Microgels as a Tool for Stimulated Spongelike Adsorption of Biomaterials for Biosensor Applications. *Biomacromolecules* **2014**, *15*, 3735−3745.

(22) Sivakumaran, D.; Mueller, E.; Hoare, T. Temperature-Induced Assembly of Monodisperse, Covalently Cross-Linked, and Degradable Poly(*N*-isopropylacrylamide) Microgels Based on Oligomeric Precursors. *Langmuir* **2015**, *31*, 5767−5778.

(23) Engel, S.; Höck, H.; Bocola, M.; Keul, H.; Schwaneberg, U.; Möller, M. CaLB Catalyzed Conversion of ε-Caprolactone in Aqueous Medium. Part 1: Immobilization of CaLB to Microgels. *Polymers* **2016**, *8*, 372.

(24) Peng, H.; Huang, X.; Oppermann, A.; Melle, A.; Weger, L.; Karperien, M.; Wöll, D.; Pich, A. A facile approach for thermal and reduction dual-responsive prodrug nanogels for intracellular doxorubicin delivery. *J. Mater. Chem. B* **2016**, *4*, 7572−7583.

(25) Uhlig, K.; Wegener, T.; He, J.; Zeiser, M.; Bookhold, J.; Dewald, I.; Godino, N.; Jaeger, M.; Hellweg, T.; Fery, A.; Duschl, C. Patterned Thermoresponsive Microgel Coatings for Noninvasive Processing of Adherent Cells. *Biomacromolecules* **2016**, *17*, 1110−1116.

(26) Kather, M.; Skischus, M.; Kandt, P.; Pich, A.; Conrads, G.; Neuss, S. Functional Isoeugenol-Modified Nanogel Coatings for the Design of Biointerfaces. *Angew. Chem., Int. Ed.* **2017**, *56*, 2497−2502.

(27) Stieger, M.; Richtering, W.; Pedersen, J. S.; Lindner, P. Small-angle neutron scattering study of structural changes in temperature sensitive microgel colloids. *J. Chem. Phys.* **2004**, *120*, 6197−6206.




DOI: 10.1021/acsomega.8b03461
*ACS Omega* 2019, 4, 3690−3699

(28) Virtanen, O.; Mourran, A.; Pinard, P.; Richtering, W. Persulfate initiated ultra-low cross-linked poly(N-isopropylacrylamide) microgels possess an unusual inverted cross-linking structure. *Soft Matter* **2016**, *12*, 3919−3928.
(29) Sheikholeslami, P.; Ewaschuk, C. M.; Ahmed, S. U.; Greenlay, B. A.; Hoare, T. Semi-batch control over functional group distributions in thermoresponsive microgels. *Colloid Polym. Sci.* **2012**, *290*, 1181−1192.
(30) Wolff, H. J.; Kather, M.; Breisig, H.; Richtering, W.; Pich, A.; Wessling, M. From Batch to Continuous Precipitation Polymerization of Thermoresponsive Microgels. *ACS Appl. Mater. Interfaces* **2018**, *10*, 24799−24806.
(31) Wu, X.; Pelton, R.; Hamielec, A.; Woods, D.; McPhee, W. The kinetics of poly(*N*-isopropylacrylamide) microgel latex formation. *Colloid Polym. Sci.* **1994**, *272*, 467−477.
(32) Gao, J.; Frisken, B. J. Cross-Linker-Free *N*-Isopropylacrylamide Gel Nanospheres. *Langmuir* **2003**, *19*, 5212−5216.
(33) Gao, J.; Frisken, B. J. Influence of Reaction Conditions on the Synthesis of Self-Cross-Linked *N*-Isopropylacrylamide Microgels. *Langmuir* **2003**, *19*, 5217−5222.
(34) Virtanen, O. L.; Ala-Mutka, H. M.; Richtering, W. Can the Reaction Mechanism of Radical Solution Polymerization Explain the Microgel Final Particle Volume in Precipitation Polymerization of *N*-Isopropylacrylamide? *Macromol. Chem. Phys.* **2015**, *216*, 1431−1440.
(35) Virtanen, O.; Brugnoni, M.; Kather, M.; Pich, A.; Richtering, W. The next step in precipitation polymerization of *N*-isopropylacrylamide: Particle number density control by monochain globule surface charge modulation. *Polym. Chem.* **2016**, *7*, 5123−5131.
(36) Virtanen, O.; Richtering, W. Kinetics and particle size control in non-stirred precipitation polymerization of *N*-isopropylacrylamide. *Colloid Polym. Sci.* **2014**, *292*, 1743−1756.
(37) Still, T.; Chen, K.; Alsayed, A. M.; Aptowicz, K. B.; Yodh, A. Synthesis of micrometer-size poly(*N*-isopropylacrylamide) microgel particles with homogeneous crosslinker density and diameter control. *J. Colloid Interface Sci.* **2013**, *405*, 96−102.
(38) Chen, Y.; Ding, D.; Mao, Z.; He, Y.; Hu, Y.; Wu, W.; Jiang, X. Synthesis of Hydroxypropylcellulose-poly(acrylic acid) Particles with Semi-Interpenetrating Polymer Network Structure. *Biomacromolecules* **2008**, *9*, 2609−2614.
(39) Li, L.; Chang, A.; Hu, Y.; Zhang, L.; Wu, W. One-pot aqueous synthesis of sub-10 nm responsive nanogels. *Chem. Commun.* **2013**, *49*, 6534−6536.
(40) de Kanter, M.; Meyer-Kirschner, J.; Viell, J.; Mitsos, A.; Kather, M.; Pich, A.; Janzen, C. Enabling the measurement of particle sizes in stirred colloidal suspensions by embedding dynamic light scattering into an automated probe head. *Measurement* **2016**, *80*, 92−98.
(41) Bressel, K.; Muthig, M.; Prévost, S.; Grillo, I.; Gradzielski, M. Mesodynamics: Watching vesicle formation in situ by small-angle neutron scattering. *Colloid Polym. Sci.* **2010**, *288*, 827−840.
(42) Keidel, R.; Ghavami, A.; Lugo, D. M.; Lotze, G.; Virtanen, O.; Beumers, P.; Pedersen, J. S.; Bardow, A.; Winkler, R. G.; Richtering, W. Time-resolved structural evolution during the collapse of responsive hydrogels: The microgel-to-particle transition. *Sci. Adv.* **2018**, *4*, No. eaao7086.
(43) Wrede, O.; Reimann, Y.; Lülsdorf, S.; Emmrich, D.; Schneider, K.; Schmid, A. J.; Zauser, D.; Hannappel, Y.; Beyer, A.; Schweins, R.; Gölzhäuser, A.; Hellweg, T.; Sottmann, T. Volume phase transition kinetics of smart *N*-*n*-propylacrylamide microgels studied by time-resolved pressure jump small angle neutron scattering. *Sci. Rep.* **2018**, *8*, No. 13781.
(44) Freltoft, T.; Kjems, J.; Sinha, S. Resolution Function and Flux at the Sample for Small-Angle X-Ray-Scattering Calculated in Position Angle Wavelength Space. *Phys. Rev. B* **1986**, *33*, 269.
(45) Pedersen, J. S.; Riekel, C. Resolution function and flux at the sample for small-angle X-ray scattering calculated in position-angle-wavelength space. *J. Appl. Crystallogr.* **1991**, *24*, 893−909.
(46) Spalla, O. General Theorems in Small-Angle Scattering. In *Neutrons, X-rays and Light: Scattering Methods Applied to Soft Condensed Matter*; North-Holland, Elsevier: Amsterdam, 2002; pp 49−71.
(47) Rubinstein, M.; Colby, R. H. *Polymer Physics*; Oxford University Press: New York, 2003; Vol. *23*.
(48) Pelton, R. Poly(*N*-isopropylacrylamide)(PNIPAM) is never hydrophobic. *J. Colloid Interface Sci.* **2010**, *348*, 673−674.
(49) Corbett, J. F. Pseudo first-order kinetics. *J. Chem. Educ.* **1972**, *49*, 663.
(50) Odian, G. *Principles of Polymerization*; John Wiley & Sons, 2004.
(51) Janssen, F. A.; Kather, M.; Kröger, L. C.; Mhamdi, A.; Leonhard, K.; Pich, A.; Mitsos, A. Synthesis of Poly(*N*-vinylcaprolactam)-Based Microgels by Precipitation Polymerization: Process Modeling and Experimental Validation. *Ind. Eng. Chem. Res.* **2017**, *56*, 14545−14556.
(52) Kröger, L. C.; Kopp, W. A.; Leonhard, K. Prediction of Chain Propagation Rate Constants of Polymerization Reactions in Aqueous NIPAM/BIS and VCL/BIS Systems. *J. Phys. Chem. B* **2017**, *121*, 2887−2895.
(53) Radulescu, A.; Szekely, N. K.; Appavou, M.-S. KWS-2: Small angle scattering diffractometer. *J. Large-Scale Res. Facil.* **2015**, *1*, A29.
(54) Riesen, R. Bilanz-reaktionskalorimetrie. *Thermochim. Acta* **1987**, *119*, 219−222.
(55) Grob, B.; Riesen, R. Reaction calorimetry for the development of chemical reactions. *Thermochim. Acta* **1987**, *114*, 83−90.



DOI: 10.1021/acsomega.8b03461
*ACS Omega* 2019, 4, 3690−3699